

The mouse retina in 3D: quantification of vascular growth and remodeling†

Cite this: DOI: 10.1039/c3ib40085a

Florian Milde,^a Stephanie Lauw,^b Petros Koumoutsakos^{†*a} and M. Luisa Iruela-Arispe^{†*b}

The mouse retina has become a prominent model for studying angiogenesis. The easy access and well-known developmental progression have significantly propelled our ability to examine and manipulate blood vessels *in vivo*. Nonetheless, most studies have restricted their evaluations to the superficial plexus (an upper vascular layer in contact with the vitreous). Here we present experimental data and quantification for the developmental progression of the full retina including the intermediate and deeper plexus that sprouts from the superficial layer. We analyze the origin and advancement of vertical sprouting and present the progression of vascular perfusion within the tissue. Furthermore, we introduce the use of Minkowsky functionals to quantify remodeling in the superficial and deeper plexus. The work expands information on the retina towards a 3D structure. This is of particular interest, as recent data have demonstrated differential effects of gene deletion on the upper and deeper plexus, highlighting the concept of distinct operational pathways during sprouting angiogenesis.

Received 6th May 2013,
Accepted 23rd September 2013

DOI: 10.1039/c3ib40085a

www.rsc.org/ibiology

Insight, innovation, integration

The mouse retina is a popular model for the study of developmental angiogenesis. We present annotated image data of the vasculature in the mouse retina throughout development and suggest metrics that quantify the emerging sprouting patterns. Furthermore, we introduce a morphological analysis based on Minkowsky functionals to capture vascular growth and remodeling. We use these methods to study angiogenesis in the mouse retina. The results present, for the first time, a comprehensive, quantitative analysis of vascular sprouting and remodeling during retinal development. The study reveals distinct sprouting patterns along the arteries, capillaries and veins of the retina and defines a landscape for vascular remodeling. The presented data can be used for the evaluation of future genetic and pharmacological perturbation studies.

Introduction

The retina is becoming a highly adopted platform to study angiogenesis, vascular morphogenesis, remodeling and differentiation.¹ In contrast to the depth covered by most vascular beds, the retinal vasculature is nearly planar, yet hierarchical and almost stereotypical. These features make it an ideal system to perturb, manipulate and rescue genetic defects. In addition, the vasculature of the retina has enabled the acquisition of significant information related to the effect of hypoxia on blood vessels.^{2–4} The exploration of this system as a model for retinopathy of prematurity and other vascular-associated

disorders has facilitated advancements from pre-clinical to clinical trials in a manner that has not been paralleled by other fields.^{5–7}

In the mouse, growth of retinal vessels initiates shortly after birth (postnatal day 1, P1) and concludes after the third week of life. The superficial vascular plexus is the first to be formed. A dense, primitive plexus with a large number of vascular sprouts is quickly established at the periphery of the expanding vascular front (P1–P3). Recurrent remodeling and pruning of this primitive plexus leads to the formation of a hierarchical network structure. The emergence of distinct vessel types, arteries and veins connected by intervening capillary beds, quickly follows through a process of progressive differentiation and differential oxygenation is then established (P5–P8) (see Fig. 1a).

As vascular remodeling commences at the centre of the retina, the primitive vascular plexus at the periphery of the retina still remains for one additional week. Thus, during the second week (postnatal) in the mouse, the retinal vasculature offers

^a Computational Science and Engineering Laboratory, ETH Zürich, CH-8092, Switzerland. E-mail: petros@ethz.ch

^b Department of Molecular, Cell & Developmental Biology, UCLA, Los Angeles, California, USA. E-mail: arispe@mcdb.ucla.edu

† Electronic supplementary information (ESI) available. See DOI: 10.1039/c3ib40085a

‡ Both authors contributed equally to this work.

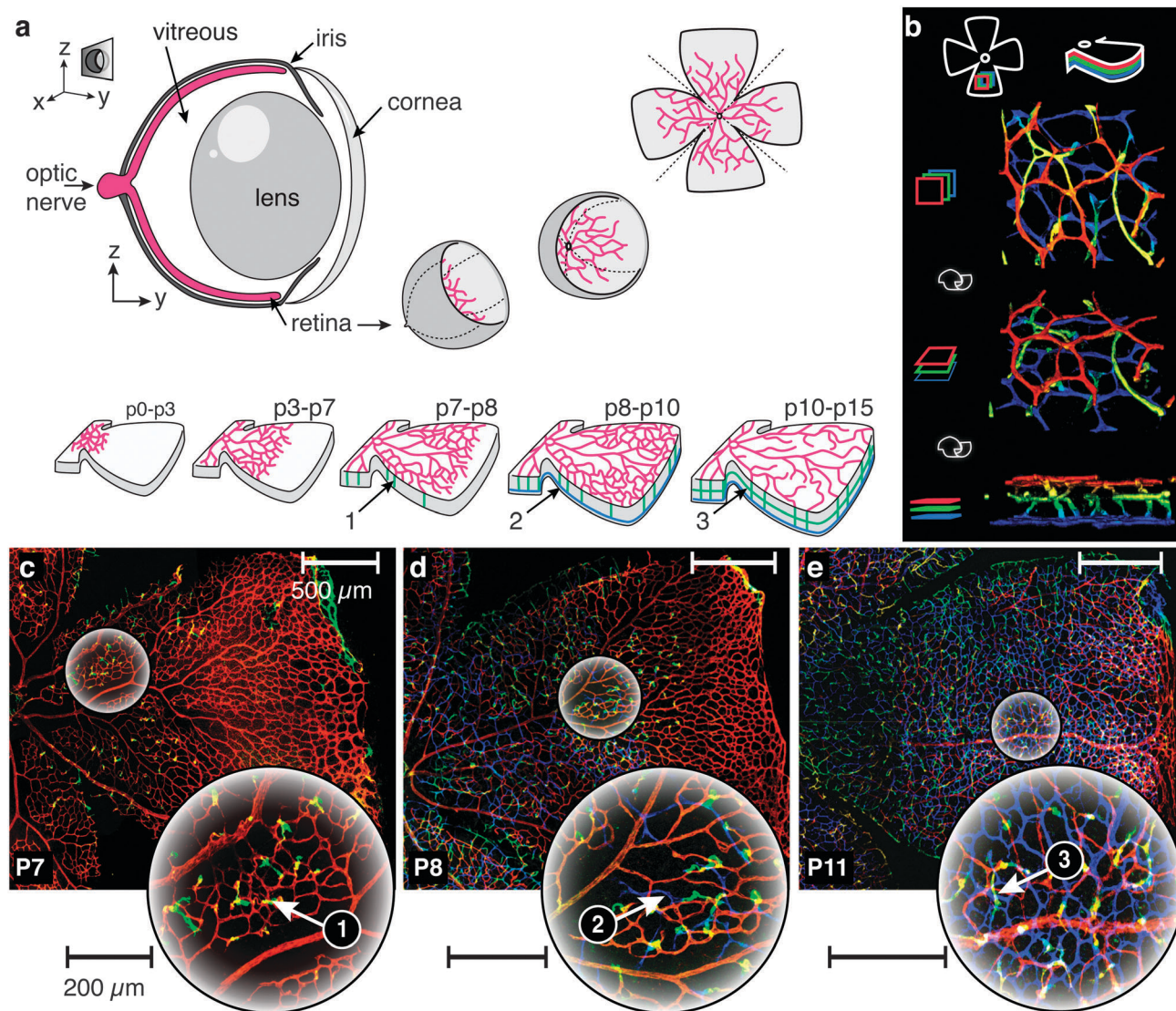


Fig. 1 The mouse retina, a model system for the study of angiogenesis. (a) Top: conceptual sketch illustrating the generation of specimens for evaluation of the vasculature. The retina cup is separated from the enucleated eye, clipped to unfold into a clover leaf-like structure, stained for endothelial cells and mounted onto a cover slip for confocal imaging. Bottom: schematic sketch of the developmental stages during retinal angiogenesis. Sprouting is initiated from the optic nerve and proceeds to cover the entire retina around P8, followed by subsequent remodeling and maturation of the superficial plexus. Vertical sprouting is observed around P7 (green, 1) followed by the formation of a second, deep plexus around P8 (blue, 2) and a third, intermediate layer around P10 (green, 3). (b) 3D reconstruction of the retinal vasculature. Colors indicate Z-stack depth: first layer (red), intermediate, third layer (green) and inner most, second layer (blue). Top to bottom: rotation from top to side view. (c–e) Vertical sprouting progression during retina vascularization. Color indicates depth (see (b)). Left to right: P7, P8 and P11. Large circular images show magnified regions indicated in the original images. (c) P7: onset of vertical sprouting into the retina (green, 1). (d) P8: formation of a second vascular layer (blue, 2) at the tip of the vertical sprouts (green). (e) P11: vertical sprouting and deeper plexus formation has progressed to cover most of the first layer. A third vascular layer (green, 3) forms between the first and the second layer.

concurrent visualization of multiple steps in the process of vascular maturation; including: sprouting, branching, fusion (in the periphery), remodeling and maturation (towards the centre).^{1,8,9}

The accessibility and characteristics described above have placed the retina as the prototypical vascular network for evaluation of transgenic mice and for pharmacological testing and intervention.^{1,10} However, most studies have focused specifically on the superficial vascular plexus; while the intermediate and deep layers have been less explored. These layers originate shortly after the initial growth of the upper (superficial) plexus.

Sprouting vertically from the mature region of the superficial plexus, new vascular sprouts invade the retina and establish a secondary, deeper layer and ultimately a tertiary vascular layer that evolves in-between the superficial and the deeper layers. The entire process is completed in about 16 days and results in the formation of an interconnected, three-dimensional network of vessels that spans the entire retina (see Fig. 1b). Labeling the endothelial cells of the retina in a depth-dependent color scheme illustrates how the progression of sprouting from the superficial plexus invades the retina and establishes this highly hierarchical, three dimensional network pattern (see Fig. 1c).

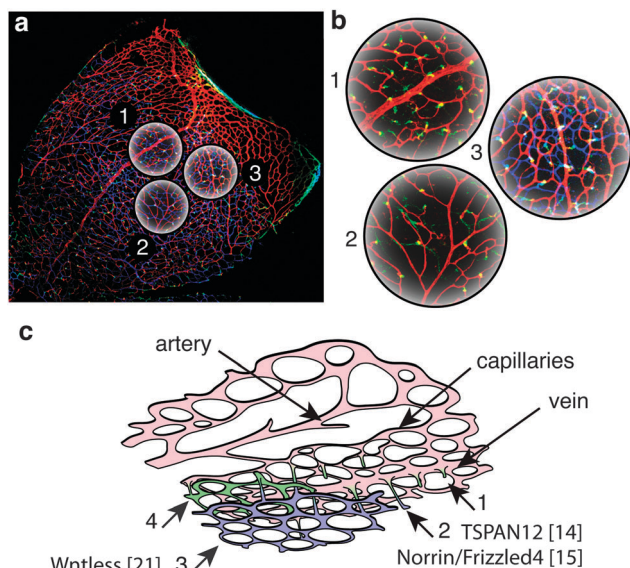


Fig. 2 Development of the deeper and intermediate layers occurs through a series of vertical sprouts from vessels located in the superficial layer. (a) P10 retina showing sprouting progression of vertical sprouting along the central vein and capillary beds. (b) Magnified regions marked in (a). Colors indicate the different layers: superficial plexus (red), sprouts (green) and the deeper layer (blue). Sprouts originate from veins and capillaries of the superficial plexus (b1, red). Sprouts do not appear on arterial vessels (b2). For better perception, the blue layer has been removed from images b1 and b2. Sprouts penetrate to reach the INL and turn sideways to establish the deeper layer (b3). (c) Conceptual sketch of the guiding mechanisms involved in deeper layer formation: initial sprouting (c1); sprouts stop at the INL (c2); formation of a secondary, deeper layer (c3); formation of a third, intermediate layer (c4).

The vertical sprouting proceeds in a controlled spatial and temporal order.¹¹ However, with very few exceptions, the precise mechanisms that control sprouting into the deeper layers are not fully understood.¹² Fig. 2 illustrates the process of vascular sprouting from the superficial plexus into the deeper layers of the retina and it indicates some of the molecules known to affect the process.^{12–14} In particular, members of the Wnt family appear to regulate the vertical sprouting process.¹⁵

Despite the apparent similarities, the superficial, intermediate and deeper vascular layers of the retina are not identical. Vascular expansion of the superficial layer is preceded by a network of astrocytes that spreads radially from the optic nerve.^{16,17} Astrocytes secrete fibronectin, critical for adequate advancement of the vascular plexus.¹⁸ The intermediate and deeper vascular layers are not associated with retinal astrocytes being exposed to distinct heterotypic cell interactions and matrix proteins. There are also clear molecular differences between the superficial, intermediate and deeper plexus. For example, deletion of TSPAN12 completely ablates sprouting into the intermediate layer and prevents the formation of the deeper layer. These severe defects occur albeit in an apparently normal, and developmentally unaltered upper plexus.¹² TSPAN12 is a chaperone for the Norrin/Fz4 signaling pathway and deletion of either Norrin or Fz4 exhibits similar defects to those of TSPAN12.^{13,19} The findings strongly indicate that the molecular mechanisms involved in the regulation of angiogenesis in the intermediate

and deeper layers are not identical to those operational in the upper plexus.

Our ability to interpret data from genetic and pharmacological modifications that expand into the intermediate and deeper layers is limited by the paucity of available information on these layers. The goal of this study was to analyze and quantify the progression of vertical sprouts over time using a large library of wild-type retinas and to develop a method to mathematically describe vascular remodeling.

Today, retina networks are commonly quantified based on features selected from confocal images. These quantifications involve distance and event-based metrics from measurements such as the number of sprouts and junctions, the length and diameter of vessels and sprouts, the percentage of vascularized area, the filopodia number and length or the number of endothelial stalk and tip cells.^{20–23} Branching patterns have also been classified by measuring the degree of branching.¹⁴

A more comprehensive quantification of network structures implies a robust and accurate segmentation of the vasculature. The automated segmentation of vessels is a well-studied topic (see review by Kirbas and Quek²⁴). Although a plethora of technologies have been developed to segment confocal laser microscopy images, we are only aware of a few studies that apply such segmentation algorithms to fluorescent images of the retinal vasculature.²⁵

Based on an accurate and detailed segmentation and skeletonization of the vascular network, a number of additional methodologies have been proposed to quantify and characterize connectivity, hierarchy and morphology in vascular networks. Next to the distance and counting based metrics, vessel tortuosity,^{26,27} fractal dimension,^{28,29} lacunarity²⁸ and branching angles³⁰ together with the corresponding methods to extract these metrics have been proposed to characterize vascular networks. Branching generation in vascular trees has been considered,³¹ however non-hierarchical network structures like the ones seen in the deeper layers of the retina vasculature cannot be analyzed with such methods.

In addition to methodological developments, the automation of these processes along with efficient software is an essential aspect of quantification. Czech and colleagues followed a graph theory approach and propose statistical and algebraic descriptors to analyze global and local structural properties of vascular networks.³² These metrics have been integrated into a software toolbox, the Graph Investigator. VESGEN 2D is another software package that offers automated, user-interactive quantification of vascular networks. The tool comprises methods to extract distance and area based metrics, the number of branch points as well as fractal dimensions and vessel tortuosity. The toolbox has showcased segmentation examples in a variety of different imaging data, including fluorescent-labeled retinal vasculature.²⁵ Finally, a computer-aided quantification method for the retinal neovascularization in pathological retinopathy has recently been introduced.^{33,34} This method focuses on the measurement of areas of neovascularization ignoring completely the generated vascular network structures.

In this work, we present novel methods and metrics for the systematic description and quantification of vascular growth

progression in the retina of the mouse. The methods comprise guidelines for the manual annotation of vertical sprouting progression, a robust network segmentation algorithm and the quantitative analysis of vascular network patterns using Minkowsky functionals.³⁵ We apply these techniques on the large database of wild-type retina images collected throughout this study and present a detailed, quantitative description of vertical sprouting and network maturation in the developing vasculature of the retina.

Materials and methods

Tissue preparation

Experiments were performed in accordance with ALAAC regulations and under UCLA approved protocols. Eyes were collected from wild-type C57Bl6 mice spanning the developmental stages from birth (P0) to postnatal day 16 (P16) and from adult animals. The eyes were first exposed to a brief fixation (3–5 min) in 2% (wt/vol) of paraformaldehyde (PFA). Retinas were then dissected from the sclera and choroid in phosphate buffered saline (PBS) and clipped to unfold into a clover like structure (Fig. 1a), additional fixation with 2% PFA followed for no longer than 16 hours. Retinas were used immediately or stored in methanol at -20°C . Prior to staining at least three washes in PBS for 10 min each were performed. Subsequently, retinas were incubated in blocking solution (0.1% Triton X-100, 1% fetal calf serum in PBS) for one to three hours at room temperature. The specimens were then exposed to Griffonia simplicifolia isolectin B4 (Vector Labs, Burlingame, CA), a pre-conjugated glycoprotein that recognizes sugars on the surface of endothelial cells and enables visualization of blood vessels. Incubation with isolectin (1:200 dilution) was done overnight at 4°C , samples were subsequently washed in PBS containing 0.1% Triton four times for 30 min each and mounted using Vectashield (Vector Labs, Burlingame, CA). A conceptual sketch of the image preparation is depicted in Fig. 1a.

Image acquisition

The specimens were imaged on a Zeiss LSM 510 multiphoton microscope ($10\times/0.45\text{NA}$) with Zen software (Carl Zeiss). We used multi-tile imaging with an x - y resolution of $1.135\ \mu\text{m}$ per pixel and a varying z resolution (5 – $9\ \mu\text{m}$) in order to capture all vascular layers of the retina. In a post-processing step, the whole-mount image stacks were cut into segments featuring single retina wings (see Fig. 1c–e). We collected a total number of 126 retina wings according to Table 1.

Image analysis and quantification

We have developed custom tailored MATLAB image processing routines for the analysis and quantification of fluorescent-labeled retinal vasculature images of the mouse. The package integrates manual annotation functionality, network segmentation routines, statistical analysis and morphological image analysis.

Table 1 Retina image database. Number of retina wings from the number of different retinas per postnatal day

Day	Wings/retinas
P0	15/6
P1	15/4
P2	7/3
P3	11/4
P4	10/3
P5	4/2
P6	10/3
P7	7/2
P8	13/4
P9	8/3
P10	6/3
P11	3/2
P12	4/2
P15	3/1
P16	1/1
Adult	9/4

Image annotation

The retina images were manually processed and annotated for landmark features of interest. These features include the total area of the retina, the area covered by the vasculature of the superficial layer, the area covered by the primitive plexus, the location of the optic nerve, traces of the main arteries and veins and the location of the vertical sprouts originating from the superficial plexus (see Fig. S1, ESI[†]). The locations of the vertical sprouts were further marked according to their location on the superficial plexus. This allowed us to distinguish sprouts emerging from veins, arteries and capillaries. A conceptual sketch of an annotated retina wing is depicted in Fig. 3a.

Vertical sprouting quantification

In order to better understand the evolution of characteristic sprouting patterns in the retina, we established a quantitative description of vertical sprouting progression during normal retina development.

Sprouting densities. We report sprouting densities with respect to the area of the retina covered by the superficial plexus. Refined sprout densities from the capillaries, veins and arteries of the superficial plexus are analyzed. In order to obtain an area estimate for these vessels, we multiply the length of the arteries and veins of the superficial plexus with a fixed clearing width of $50\ \mu\text{m}$ ($25\ \mu\text{m}$ to each side). This area reflects the vascular clearing area around arteries and veins observable in the confocal images (see Fig. 1c–e). The area of the capillaries is defined as the area covered by the superficial plexus minus the area covered by the veins and arteries.

Spatial sprouting progression. We further report the spatial sprouting progression over time. The superficial plexus is binned into 10 bins of uniform width at an increasing distance with respect to the optic nerve. A sprouting density is calculated per bin.

Network maturation and sprouting. We relate the sprouting progression to the remodeling and maturation advancement in the superficial plexus. We estimate the area covered by sprouts and calculate their size and overlap with respect to the remodeled fraction of the superficial layer and the primitive plexus at the

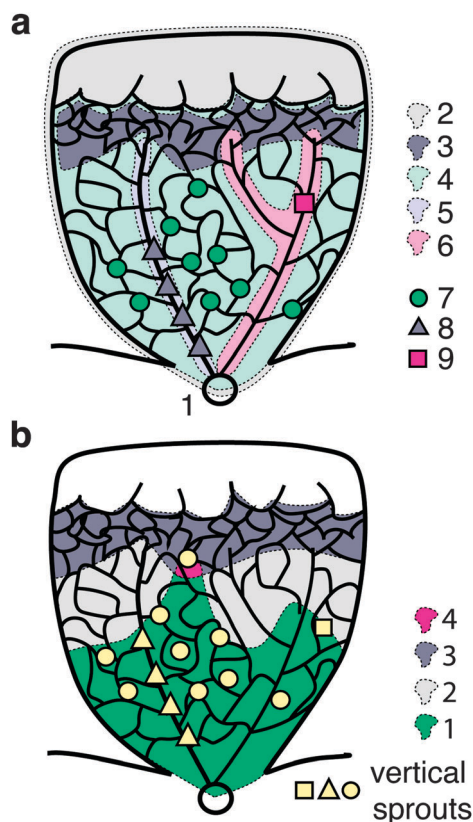


Fig. 3 Retina image annotation. (a) Conceptual sketch of the retina image preparation for sprouting quantification. Individual datasets consist of isolated retina wings. The position of the optic nerve (a1), retina mask (a2), primitive plexus mask (a3), vessel network mask (a4), traces of the main veins (a5) and arteries (a6) are marked by hand. Vertical sprouting positions are marked and labeled according to their origin in the superficial plexus: capillary bed (a7), vein (a8) and artery (a9). (b) Schematic sketch of the masking of sprout coverage (green, b1), primitive plexus (dark gray, b3) and their overlap region (pink, b4). Light gray regions represent the differentiated portion of the first layer not covered by sprouts (b2).

periphery of the retina. A conceptual sketch of the region fractions is given in Fig. 3b.

Sprout space partition. We further investigated the partition of space as defined by calculating a Voronoi tessellation^{28,36} around the sprout locations. Along with the Voronoi diagram, we also obtain the Delaunay triangulation of the sprouts that allows us to extract inter-sprout distances (see Fig. S4, ESI†).

The sprouts are classified into 3 groups determined by the association of the Voronoi region of every sprout and the pattern of the superficial plexus. Sprouts are classified as venous (V) sprouts, if they originate from a vein and arterial (A) sprouts, if the Voronoi region overlaps with an artery, effectively labeling the sprouts lining arteries. The remaining sprouts that originate from the capillary bed are labeled capillary (C) sprouts. The Voronoi regions capture the perfusion area associated with the individual sprouts, as they define areas that are closer to the corresponding sprout than to any other sprout.

Network segmentation

The networks of the superficial plexus were segmented using a semi-automated, multi-stage segmentation algorithm. Uneven

illuminations in the original image were estimated and removed based on morphological opening of the original image. A curvelet analysis was conducted and features of small scales were removed in curvelet space,^{37,38} producing a de-noised image that preserves the characteristic, elongated vessel structures. A locally adaptive threshold map was employed for threshold-based segmentation. The spatially adaptive threshold level accounts for the elevated background fluorescence in the primitive plexus at the sprouting front and produces robust segmentation results (see Fig. S2, ESI†).

Quantifying network morphology

The segmented vascular network was quantified based on morphological analysis and Minkowsky functionals.³⁵ In two dimensions, Minkowsky functionals are represented by three additive image functionals that describe the morphological content of a two dimensional pattern by its area, perimeter and the Euler characteristic (the number of connected objects minus the number of enclosed islets) (see Fig. S3, ESI†). For simplicity, we will refer to them as area, perimeter and inter-vascular spaces throughout this article. These metrics are captured as the binary pattern is subject to image dilation, a process in which the object is expanded in the direction orthogonal to its boundary. This produces a functional representation of a binary pattern in the three Minkowsky metrics. A schematic sketch of this process is depicted in Fig. 4. To allow for comparison among images of varying size, the image functionals are normalized with the total area of the retina wing.

Geometric analysis with Minkowsky functionals offers a powerful alternative to quantitative analysis of a selective, limited number of distinct network properties. The functionals

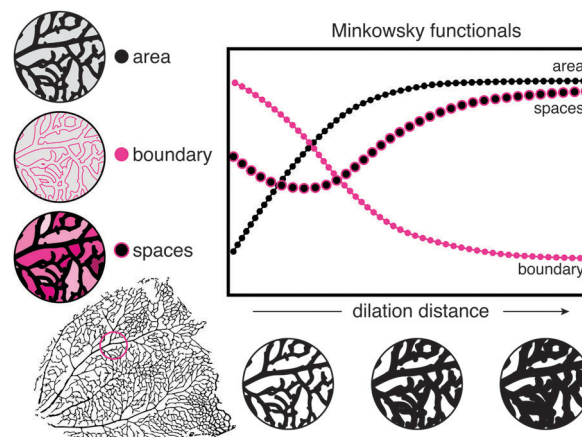


Fig. 4 Evaluating vascular remodeling with Minkowsky functionals. Analysis of Minkowsky functionals for the retinal vasculature of the first layer depicted in the lower left corner. Top left: Minkowsky metrics: area size, boundary length and the Euler characteristic (the number of connected objects minus the number of enclosed spaces) denoted as intervascular spaces. All numbers were normalized to the total area of the retina wing. Top right: Minkowsky functional representation of the retina vasculature. Area, boundary and intervascular spaces are reported as functions of the dilation distance of objects. Bottom right: magnified region (pink circle) of the network subject to morphological dilation.

Table 2 Morphological interpretation of the slopes in the Minkowsky functionals with respect to vascular networks

Metric	Slope	Sign	Morphologic interpretation
Area	Flat	+	Many branches, small intervascular spaces, tortuous vessels
	Steep		Few branches, large intervascular spaces, straight vessels
Boundary	Flat	–	Simple structure, few branches
	Steep		Complex structure, many branches
Spaces	Flat	+	Round lacunas, large variation in lacuna size
	Steep		Elongated lacunas, lacunas of similar size
	Flat	–	Sparse tree, few blind ends located far away from other vessels
	Steep		Dense tree, many blind ends close to other vessels

capture the morphological content of a network in only three curves. The approach is unbiased towards vascular networks, well supported by mathematical theory and the functionals are easily interpretable, as they have a direct geometrical meaning (area, boundary, spaces). Capturing these properties as the image is dilated allows for a sophisticated interpretation of the data. The slopes in the area, perimeter and the Euler characteristic subject to dilation, and their relation to each other, reveal structural properties of the analyzed networks (see Table 2). These observations at increasing dilation distances differentiate between the small and large-scale features in a network. Most importantly, the functionals can capture and quantify differences among distinct network topology without the subjective selection of preferential metrics.

Results

We generated a database consisting of 126 retina wing images from 47 different retinas at developmental time points spanning the range from postnatal day 0 (P0) to P16, as well as fully vascularized retinas from adult animals (see Table 1). These samples were used to compile detailed information on angiogenic progression, remodeling and expansion of the intermediate and deeper vascular layers.

Progression of vertical sprouting

Vertical sprouting from the superficial plexus is initiated around P7. A steady increase in the mean sprouting density follows from the vascularized upper plexus, saturating around P15. The data up to this point suggest a sigmoidal saturating curve. For adult retinas, we observed a decrease in sprouting density by ~35% as compared to the maximal sprout density seen at P15 (Fig. 5a). This decrease has been attributed to remodeling processes taking place mainly in the superficial plexus. By pruning of capillaries in the first layer, some of the vertical sprouts lose their connection to the upper plexus and regress as well. This hypothesis is supported by the presence of open-ended sprouts extending from the deeper layers towards the superficial plexus in P15 retinas (not shown). Alternatively, a persistence of ocular growth after the establishment of a mature retinal vasculature could account for a decrease in the mean sprout density. We noted that the two mechanisms are complementary and could together account for the decrease in the mean sprout density in the adult animal.

We further investigated the frequency of sprouting from distinct vessels in the superficial plexus and observed that sprouts emerge almost exclusively from veins and the capillary beds (see Fig. 5b). The sprouting from capillaries seems to closely follow the sprouting from veins. Furthermore the sprout density on veins is saturated around P10 whereas the number of sprouts per area in the capillary beds continues to increase until P15. We noted that sprouts on both capillaries and veins are subject to pruning and remodeling from P15 until adulthood at a comparable rate.

The onset of sprouting can be localized at a distance of approximately 20% into the vascularized area of the retina, extending up to 50% into the vascular plexus (see Fig. 5c). After initiation, sprouting progresses radially outwards and reaches the peripheral border of the vascular network around P9. We found a refinement/remodeling of the sprouting density throughout the complete retina until P15, where we calculated the highest sprouting density of 2.3×10^{-4} sprouts per μm^2 at the outer rim of the retina. Over time, pruning of the vertical branches remodels the sprouting pattern to show an almost constant density of 1.4×10^{-4} sprouts per μm^2 throughout the whole retina. The increase in sprout density towards the rim of the retina from P11 through P15 indicates that sprouting has advanced to cover the entire retina. However, maturation of the superficial plexus and the successive pruning of the vertical branches have not advanced to the outer most regions of the vasculature yet. Extensive remodeling of the peripheral network region will lead to the observed regression in sprout density as the network matures.

In Fig. 5d, we report the area of the superficial layer that has exhibited vertical sprouting and relate this area to the regions of the plexus that have experienced remodeling and maturation. A conceptual sketch of the region fractions quantified in Fig. 5d is given in Fig. 3b. The data indicate that sprouting occurs exclusively from the superficial layer that has been already subject to remodeling. Minor overlap of the superficial plexus and the sprouting region is only detected at time points past P10, where remodeling has extended to cover ~95% of the first layer. In addition, the figure conveys the temporal and spatial progression of network remodeling during vascular development. The data indicate that vertical sprouting from the superficial layer is only possible after remodeling has occurred.

Considering the Voronoi tessellation around the sprout locations and the Delaunay triangulation of the sprouts, we

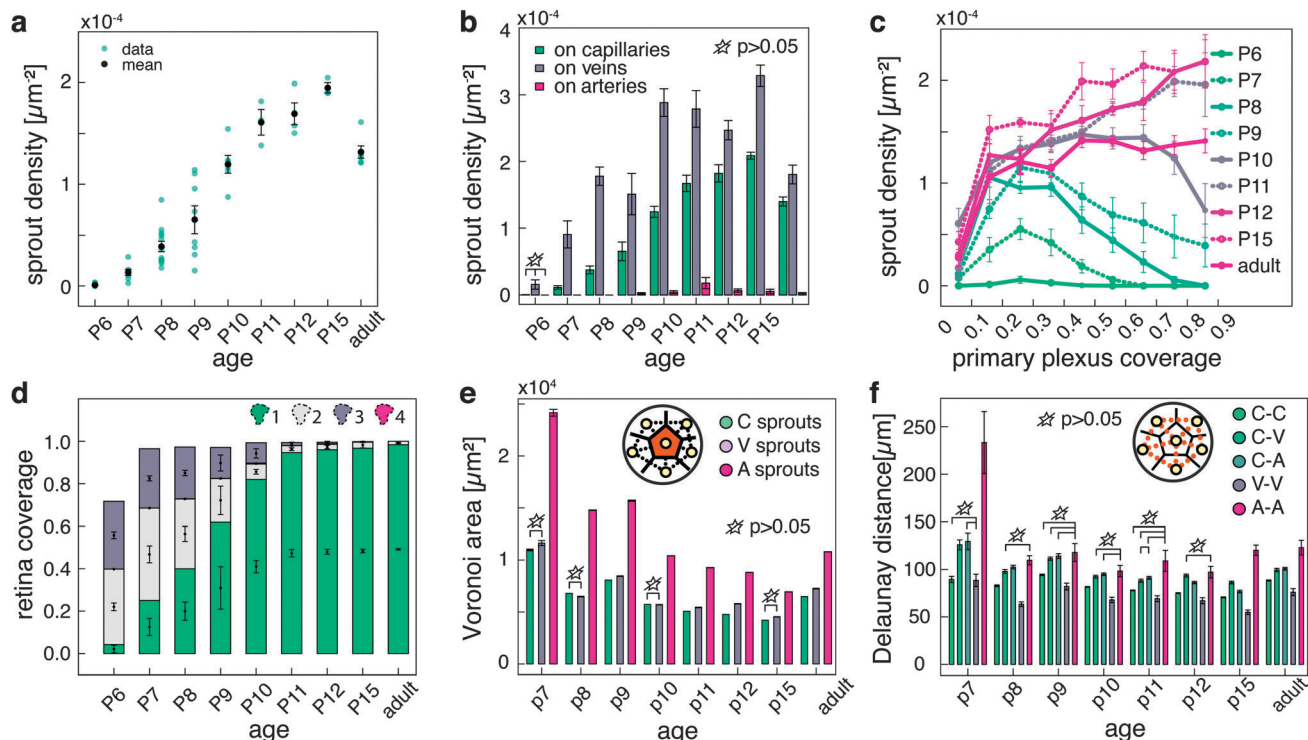


Fig. 5 Quantitative analysis of vertical sprouting progression. (a) Sprout density (number of sprouts per area) versus age. Green: individual datasets, black: mean values. (b) Sprouting density originating from capillary beds (green), veins (dark gray) and arteries (pink) versus age. Sprouting densities are reported with respect to the total area covered by the vascular network of the first layer (a) or the area covered by the arteries, veins and the capillary beds (b). (c) Sprouting progression with respect to the distance to the optic nerve. Distances are normalized against the maximal extent of the superficial plexus (x -axis). Plots (a–c) correspond to the sketch depicted in Fig. 3a. (d) Sprout coverage of the first layer in relation to network maturation versus age. Areas are normalized to the total area covered by the first layer. Plot (d) corresponds to the sketch reported in Fig. 3b. (e) Voronoi region sizes for sprout areas overlapping with capillaries (C sprouts), veins (V sprouts) and arteries (A sprouts). (f) Inter sprout distances spanned by Delaunay triangulation in between C, V and A sprouts. All error bars show s.e.m. (a, e, f). All results reported in these figures are significant, unless indicated by crossed stars ($p > 0.05$, Kolmogorow–Smirnow-test).

extract the perfusion area associated with individual sprouts together with the inter-sprout distances. We differentiate between sprouts originating from the capillary bed (C), sprouting from veins (V) and sprouts lining the arteries of the superficial layer (A) (see Fig. S4, ESI†).

From the Voronoi region size distribution, it can be seen that the area defined by A-sprouts is significantly larger than for the C- and V-sprouts. This indicates a clearing area of sprouts around arteries (see Fig. 5e). This can be attributed to the absence of sprouts on arterial vessels and the presence of avascular zones around the main arteries of the retina. These findings are underlined when considering the mean inter-sprout distances as revealed by the Delaunay triangulation (see Fig. 5f). Although the perfusion area for C sprouts and V sprouts is comparable, the inter-sprout distance on veins is clearly smaller than in the capillary beds, indicating a clearing area around the veins where less sprouting is observed as compared to inside the capillary beds.

Quantifying network morphology during maturation

To quantify the angiogenic progression inside the retina, we need a metric reflecting changes in a growing vasculature that is subject to both remodeling and maturation. This metric must capture the maturation stage of the network and distinguish the

developmental stage based on specific features in the network morphology. Furthermore, it should be possible to measure distances between different retinas to quantify discrepancies in temporal growth, progression and deviations in network morphology. Here we introduce Minkowsky functionals (see Fig. 4) as metrics to integrate, in a quantitative fashion, the three parameters that biologically define vascular remodeling. These are: (1) changes in vascular caliber; (2) pruning of vascular segments resulting in reduced vascular density and (3) emergence of arteries and veins. The application of Minkowsky functionals allows us to compare the growth progression and morphological differences in the three vascular layers of the retina concurrently. We provide a segmentation image of the three network layers in an adult retina, together with the mean Minkowsky functionals for the network area (A), boundary length (B) and the intervascular spaces (S), for the three layers, averaged over seven retina wings (see Fig. S5, ESI†). The network images indicate a striking difference in morphology contained inside the three images. Considering the corresponding functionals A, B and S, we see that not every functional is equally capable of capturing these differences in network morphology. Whereas the vessel area (A) seems to follow a very similar curve, at least for the first and the second layer, differences are clearly captured in the intervascular spaces (S). The figure suggests that together, the functionals are

well suited to capture morphological differences in planar vascular networks.

As our objective is to use Minkowsky functionals to quantify remodeling of a vascular plexus undergoing maturation, the method needs to be sensitive enough to capture differences in networks of similar age and correctly reflect their temporal ordering. In Fig. 6a and b, we present characteristic segmentation images of the superficial plexus at three different developmental stages (P6, P12 and adult), together with the mean Minkowsky functionals over a number of retina wings (see Table 3) for the time-points P6, P8, P12 and the adult retina. Clearly, the metrics are responsive enough to capture the

morphological differences in the superficial plexus at different remodeling stages. Moreover, the functional representation directly reveals morphological properties of the network in the three observed metrics.

Comparing the networks at early and late stages, the shift in the mean area curve (Fig. 6b, 1) provides us with a mathematical function that reflects remodeling. This term encompasses the removal or thinning of vascular segments, as the nominal area covered by the endothelial cells of the vascular network decreases. The corresponding delay in the collapse of the mean boundary length of the networks subject to dilation (Fig. 6b, 2) reveals the replacement of small network lacunas by bigger

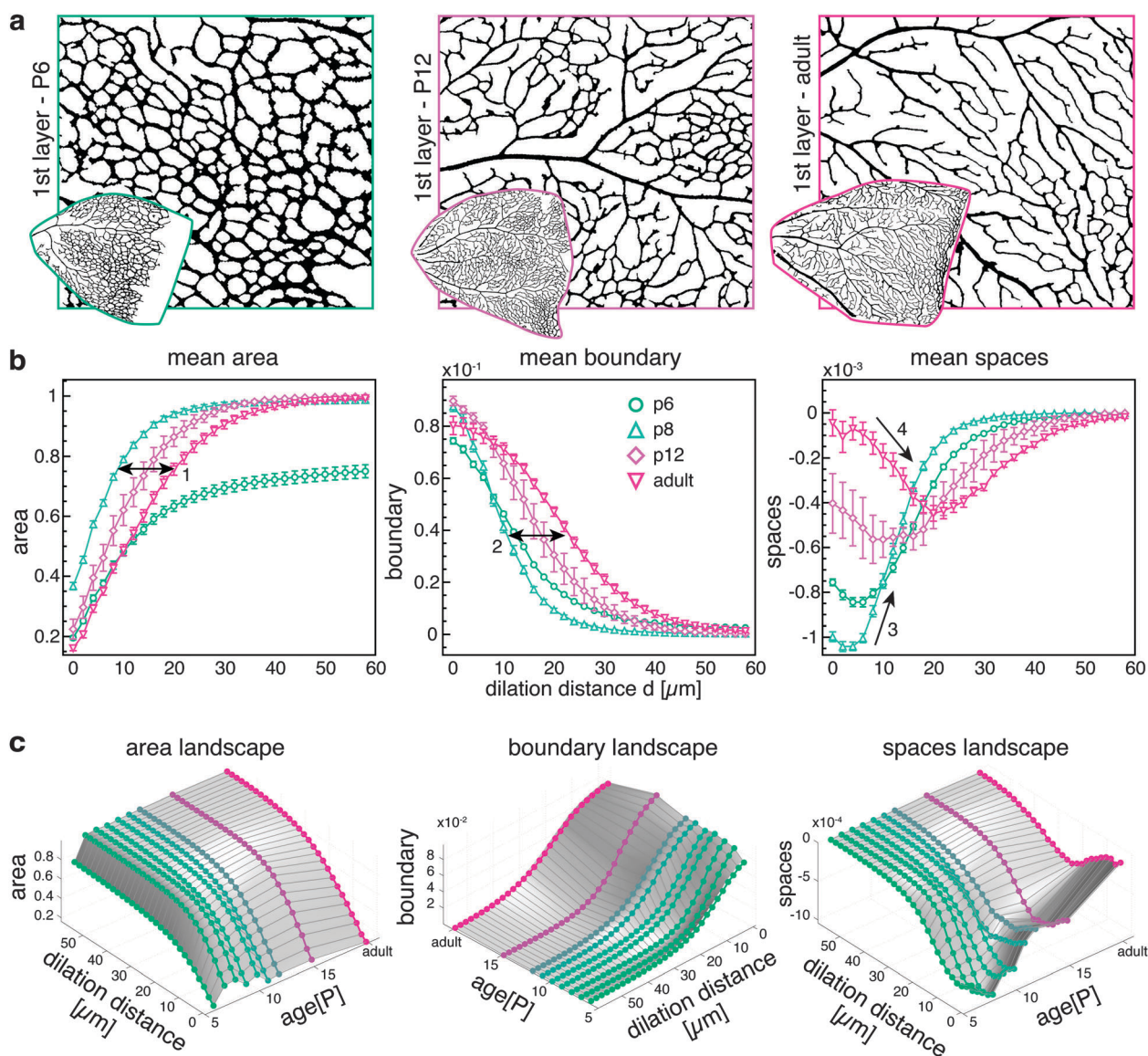


Fig. 6 Quantifying vascular remodeling using Minkowsky functionals. (a) Segmentation images of the superficial vascular layer in a P6 (left), P12 (center) and an adult retina (right). Large images show a magnified section of the retina wing (bottom left). (b) Mean Minkowsky functionals for the area (left), boundary (center) and intervascular spaces (right) metric (see Fig. 4) for P6, P8, P12 and adult retina wings. Arrows depict (b1) shift in mean total area covered by the vasculature, (b2) shift in mean boundary length of the vasculature and (b3, b4) change in slope of the mean intervascular spaces metric as the vascular network matures. (c) Minkowsky landscapes for the three Minkowsky functionals. All metrics were normalized with the total area of the retina wing. Means were estimated for $n = 10$ (P6), $n = 11$ (P8), $n = 3$ (P12) and $n = 5$ (adult) retina wings (see Table 2). Error bars represent s.e.m.

Table 3 Retina image database used in maturation path estimation. Number of retina wings from the number of different retinas per postnatal day

Day	Wings/retinas
P6	10/3
P7	6/2
P8	11/4
P9	4/3
P10	3/2
P11	2/2
P12	3/2
P15	3/1
P16	1/1
Adult	5/3

ones. This observation suggests that the decrease in area is a result of branch removal that leads to a collapse of lacunas, rather than a thinning of individual vessels. Ultimately, the change in the slopes of the intervascular spaces metric for adult retinas as compared to not fully matured vascular networks highlights the difference in the specific network structure, reflecting the emergence of arteries and veins (Fig. 6b, 3 & 4). Whereas an initial increase in this metric indicates a network-like structure that quickly fills up intervascular spaces as the image gets dilated (3), a decrease in this metric (4) indicates the partition of existing lacunas into smaller ones as a result of image dilation. This points to a tree-like network structure, as open-ended sprouts are dilated to join nearby vessel walls, partitioning one lacuna into two.

Most importantly, we can identify a trend that the functionals follow as the networks grow and mature with age. The mean Minkowsky functionals for the retinas of different age can thus be assembled to represent a surface over the space spanned by the dilation distance and the retina age (see Fig. 6c). Together, these surfaces define a maturation landscape (ML) that mathematically describes vascular network remodeling in the Minkowsky spaces and can be used as a reference for studies of maturation progression and deficiencies.

Estimating developmental age from morphology

When harvesting mouse retinas, the age of the retina is estimated based on the recorded birth age of the mouse. We refer to this estimated age as the chronological age of a retina. The chronological age is subject to an error of ± 1 day due to developmental differences associated mostly with access to nutrients and oxygen. Accordingly, also the harvest time of a retina is recorded at the granularity of days, which can add another error of ± 1 day to the mouse's real age. Together, this protocol can introduce an error of up to two days in the estimation of the retina's chronological age.

Next to the chronological age of a mouse, a developmental age can be defined based on the mouse's progression stage along its path towards maturity. Even if the chronological age of a mouse could be determined exactly, variations between this estimate and a mouse's developmental age exist as a result of premature birth or overdue pregnancy. Furthermore, the development of a mouse at an early age can vary greatly due to differential access to nutrients with respect to its littermates

postnatally or as a direct consequence to a treatment/genetic alteration. A direct feedback loop as a result of advanced development and the competition for nutrients can further amplify these differences.

Whereas we expect such variations to filter out by calculating averages over a large set of data, these discrepancies in chronological and developmental age can become problematic in the analysis of small datasets, typical for genetic experiments that require multiple transgenes in the same mouse.

Variations in the retina data can be readily observed in the surface fit through the mean Minkowsky functionals of the retinas plotted against the chronological age (see Fig. 6c). If indeed Minkowsky functionals capture remodeling/maturation progression, as we claim they do, we would expect to see a smooth surface that reflects a maturation landscape in the Minkowsky space. Although a large variation should be filtered out by taking the mean over datasets of the same age, the surface reflects inconsistencies in this assumption, especially observable for the time points P12 and P15 in the intervascular spaces metric. We attribute these inconsistencies to discrepancies in chronological *versus* developmental age estimation. Considering the data we present for vertical sprouting progression (Fig. 5), we observe a similar inconsistency in the sprouting density between P11 and P15 along with a large variation in the data at earlier time points (around P9).

In order to account for such effects when comparing vascular development in the retina, we propose a method to estimate a mouse's developmental age based on morphological features in the retina vasculature. In essence, the algorithm we propose searches for a reordering of the retinas, based on their representation in Minkowsky space, that produces a smooth surface representation of the maturation landscape fitted to the reordered data, and thus preserves a developmental progression order in the dataset. The presented results are conducted on a subset of retina wing images as reported in Table 3. In the following, an outline of the procedure that determines the reordering of the retinas is given (Fig. 7). For a detailed description of the algorithm we refer to the ESI.†

We chose to represent each retina by the values of its Minkowsky functionals evaluated at three distinct dilation distances. For each retina, this defines a point in a 9D sub-space (three functionals evaluated at three distinct points). We then fit a curve through this point cloud and project the position of each retina onto this curve. The section of the curve containing all projected points defines the 'Maturation Path' (MP). Its origin is defined as the boundary of the section with the retinas reflecting early time points, its end is defined by the other boundary (see Fig. 7c).

The location of each projected point along the maturation path defines an ordering among the retinas together with a distance, the 'Developmental Distance' DD, from the origin of the MP. The DD is a non-dimensional distance in the 9D Minkowsky sub-space. Ordering the Minkowsky functionals of the retinas according to their DD, we can again fit a maturation landscape to the rearranged data (see Fig. 7b and d). We performed Covariance Matrix Adaptation (CMA) based

parameter optimization³⁹ to find the three evaluation points along the dilation distance that generate a reordering of the retinas which leads to the smoothest fit of a maturation landscape.

Along with the maturation path, we define a mapping from the developmental distance DD to the developmental age P' (see Fig. 7e). The mapping is defined by a function fit to the data tuples $[DD_i, P_i]$ where DD_i defines the developmental distance of retina i and P_i defines its chronological age.

In order to assess the quality of the developmental age estimate P' against the chronological age estimate P , we fit the data previously reported in Fig. 5d with a Cumulative growth curve (CGC) (see Fig. 7f). In comparison, we fit the

same data plotted against the developmental age estimate P' (see Fig. 7g). As a CGC, we choose the Chapman–Richards function defined as: $y = k(1 - e^{-(x/c)^b})$. The figures depict the fitted functions along with the confidence in the fitting as reported by the goodness of fit (r^2 value). As the reported data are the result of a coordinated growth process, it should be well describable by a cumulative growth curve.

Comparing the two plots, we observe that the CGC function fit to the area fraction subject to remodeling (2) and the total area fraction covered by vessels (3) against the estimated developmental age P' gives rise to a higher r^2 as compared to the fits to the chronological age P (r^2 : 0.889/0.893(P) vs. 0.931/0.965(P')). This indicates that the reordered data can better be

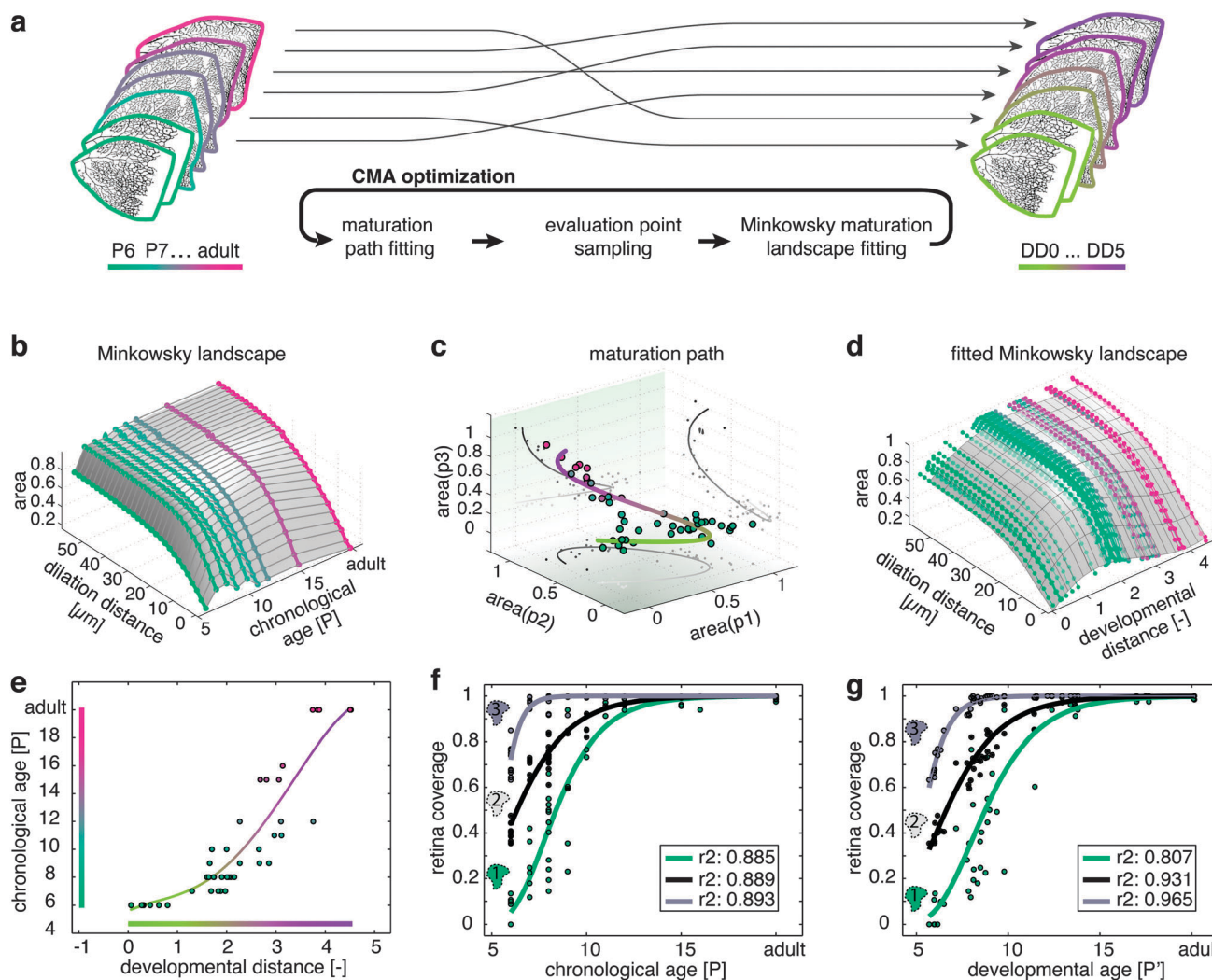


Fig. 7 Developmental maturation landscape. (a) Conceptual sketch of the optimization process that predicts the maturation path and the developmental distance among different retina wings. (b–d) Maturation path estimation depicted in the area metric. (b) Chronological maturation landscape (surface). Color indicates chronological age (green: P6, pink: adult). (c) Maturation Path estimation (colored line). Color indicates developmental distance along the maturation path from the youngest network (green: close, purple: far). Colored circles represent data points, color indicates chronological age (green: P6, pink: adult). (d) Developmental maturation landscape (surface) together with the functional representation of the individual retinas (colored lines). Color indicates chronological age (green: P6, pink: adult). (e) Mapping of the development distance to the chronological age. Circles indicate individual retinas. (f, g) Cumulative Growth Curve (CGC) function fit to the retina area fraction covered by sprouts (1, green), retina area subject to remodeling (2, black) and the retina area fraction covered by vessels (3, gray). Lines depict area fraction fits against the chronological age P (f) and the developmental age estimate P' (g). Colors correspond to sketch in Fig. 3b. Data correspond to data reported in Fig. 5d.

explained by a cumulative growth process than the original data, suggesting that the developmental age captures the progression of network growth and maturation with less variance than chronological aging. Considering the overall low confidence in the fitting of the sprouting area fraction (r^2 : 0.885(P) vs. 0.807(P')) reveals that the sprouting area progression might not behave as a cumulative growth process. Indeed, the reported results on sprouting progression in Fig. 5c have shown that vertical sprouting does not proceed in a strictly radial fashion and is subject to repeated refinement and pruning.

Conclusion

We present a quantification of the murine retinal vasculature using accurate measurements on the development and maturation of its intermediate and deeper vascular layers. These measurements complement the large body of data already available for the superficial vascular layer. The combination of these data with novel quantification tools has enabled unique insight into the development of the retina. Furthermore, we provide a library of wild-type metrics that can be used for comparisons to retinas with genetic and/or pharmacological perturbations. We introduce Minkowsky functionals to effectively quantify and describe the remodeling in all three vascular layers.

The mouse retina has quickly become the preferred platform for studies of vascular development generated from the ever-growing wealth of genetically altered mouse models.^{20,40} However, very few studies have incorporated analysis of the additional vascular layers, given the remarkable convenience of the planar structure of the superficial plexus. Interestingly, when evaluated in detail, some studies have revealed clear molecular differences between the layers. In particular, the *Norrin/Fz4* pathway is critical to mediate invasion of the vertical sprouts from the superficial layer and generation of a trilayered vascular structure.^{12,13,15}

The process of sprouting into the inner plexus is still unclear. The predicted guiding mechanism was attributed to the release of VEGF from cells of the inner nuclear layer (INL) and the sprouting location has been shown to correlate with the presence of Müller cells.²³ In fact, stability and function of the intermediate and the deeper layer also require Müller cells. Interestingly, Müller cells secrete *Norrin*¹⁹ and ablation of these cells in the adult retina results in vascular telangiectasis and dysfunction of the blood-retinal barrier.⁴¹ In addition, R-cadherin plays a role in stopping the sprouting process at the INL, preventing it from entering the sub-retinal space.¹¹ More recently, a number of mutant mouse lines have shown failure or defects in the development of the deeper layers.^{12,42–44} Although the progression of vascular expansion in all three layers of the retina typifies classical angiogenesis,⁸ the differential defects in alternative vascular layers indicate unique/specific signaling programs.

Our studies revealed that the process of sprouting from the superficial plexus into the retina is highly systematic. Vertical sprouting is initiated at P6 but exclusively from the remodeled areas of the superficial plexus. Sprouting was never found to originate from immature/not remodeled vessels. While the first

vertical sprouts are noted to emanate from veins, capillaries are equal contributors to the process. In contrast, arteries rarely give rise to sprouts. Maximum sprouting density is achieved by P15, however this density decreases in the adult, likely from remodeling of the upper plexus.

The data for vertical sprouting progression and retina vascularization have been compared to measurements reported in the literature (see Fig. S7, ESI†). Vertical sprout densities are slightly lower as compared to reported values^{12,14} (see Fig. S7a, ESI†). We note that the referenced data have been conducted on isolated sections of the retina and do not account for the area around the optic nerve that experiences little to no vertical branching. The trends in the referenced data, however, agree well with the sprouting progression reported in this work.¹⁴ The data for the superficial network progression follow closely the values reported in the literature^{19,21,45–48} (see Fig. S7b).

As vascularization proceeds, the growing inner retina becomes quickly partitioned by vertical vascular sprouts that provide oxygenation and nutrients to the nearby tissue. We used Voronoi tessellation and Delaunay triangulation to obtain an accurate measurement of the tissue areas between sprouts and to better understand the relative distances between vascular sprouts.

We found that although the mean inter-sprout distance along veins is considerably smaller as compared to inside the vascular beds ($\sim 80 \mu\text{m}/90 \mu\text{m}$ in the adult animal), the perfusion areas associated with these sprouts are very similar in size ($\sim 7000 \mu\text{m}^2$ in the adult animal). The data further indicate that the perfusion area inside these regions is homogenized *via* an increase in the sprouting distance in capillary regions alongside the veins. A similar homogenizing effect in the perfusion area of sprouts lining the arteries cannot be observed and the clearing area of capillaries along the arteries of the primary plexus is reflected in both the perfusion area and the inter-sprout distance of these vessels.

A critical event in the morphogenesis of any vascular bed is “remodeling”. The process is remarkably complex and it requires a large number of genes and interacting signaling pathways. Given these demands it is not surprising that a very large number of genetically altered mice exhibit defects in vascular remodeling and frequently succumb to death prior to the differentiation of the superficial plexus.

The term “vascular remodeling” is used to describe the events that result in the transformation of the homogeneous primitive plexus into the prototypical hierarchic vascular tree. In developmental terms remodeling includes three major cellular events: (1) changes in vascular caliber, with formation of a hierarchic vascular tree; (2) pruning of vascular segments and (3) differentiation of arteries and veins, resulting in more and less oxygenated areas and the emergence of “avascular” spaces, particularly around the arteries. Metrics to assess vascular remodeling do not exist currently. We introduced Minkowsky functionals to capture these three biological outcomes within the unifying framework of integral geometry. The approach presented herein offers significant advantages including a Minkowsky landscape representation that quantifies maturation

progression and provides the ability to estimate the developmental age of retina leaves.

The functional representation of the vascular network in Minkowsky space has been shown to distinguish hierarchical tree-like and homogeneous web-like network structures as pertinent to networks at different developmental stages. Combined, the changes in area, perimeter and Euler characteristic subject to network dilation reveal the mechanisms at work during network remodeling and maturation. We provide a maturation landscape that captures maturation progression in a quantitative fashion that can directly be linked to the changes in network topology as a result of vascular growth, pruning and differentiation. Based on this theory, we propose a methodology and a mapping function that allow for the estimation of developmental stage of retina leaves based on the morphology of its vasculature.

Currently there are few studies that offer rigorous and integrative quantification on vascular parameters. Computer-aided assessments of vascular growth/regression have only been developed for evaluation of oxygen-induced retinopathy.³³ The study presented here provides metrics that can be used for evaluation of future analysis of genetic/pharmacological perturbations. We also included unconventional approaches for the assessment of vascular remodeling changes. The findings here also offer parameters for the calibration and datasets for the validation of computer models that mimic and predict vascular growth.

Acknowledgements

FM wants to thank Dr Panagiotis Angelikopoulos for helpful discussions on Minkowsky functionals. This work was supported by Swiss National Science Foundation (to PK) and by the UC Lab Fees (to MLIA).

Notes and references

- 1 A. Stahl, K. M. Connor, P. Sapieha, J. Chen, R. J. Dennison, N. M. Kraah, M. R. Seaward, K. L. Willett, C. M. Aderman, K. I. Guerin, J. Hua, C. Lofqvist, A. Hellstrom and L. E. H. Smith, The Mouse Retina as an Angiogenesis Model, *Invest. Ophthalmol. Visual Sci.*, 2010, **51**, 2813–2826.
- 2 X. L. Gu, S. Samuel, M. El-shabrawey, R. B. Caldwell, M. Bartoli, D. M. Marcus and S. E. Brooks, Effects of sustained hyperoxia on revascularization in experimental retinopathy of prematurity, *Invest. Ophthalmol. Visual Sci.*, 2002, **43**, 496–502.
- 3 L. E. H. Smith, Pathogenesis of retinopathy of prematurity, *Growth Horm. IGF Res.*, 2004, **14**, S140–S144.
- 4 L. E. H. Smith, E. Wesolowski, A. McLellan, S. K. Kostyk, R. Damato, R. Sullivan and P. A. Damore, Oxygen-Induced Retinopathy in the Mouse, *Invest. Ophthalmol. Visual Sci.*, 1994, **35**, 101–111.
- 5 D. Kennedy, Breakthrough of the year, *Science*, 2006, **314**, 1841.
- 6 M. I. Dorrell, E. Aguilar, L. Scheppke, F. H. Barnett and M. Friedlander, Combination angiostatic therapy completely inhibits ocular and tumor angiogenesis, *Proc. Natl. Acad. Sci. U. S. A.*, 2007, **104**, 967–972.
- 7 I. S. Mantagos, D. K. Vanderveen and L. E. H. Smith, Emerging Treatments for Retinopathy of Prematurity, *Semin. Ophthalmol.*, 2009, **24**, 82–86.
- 8 M. Fruttiger, Development of the retinal vasculature, *Angiogenesis*, 2007, **10**, 77–88.
- 9 M. I. Dorrell and M. Friedlander, Mechanisms of endothelial cell guidance and vascular patterning in the developing mouse retina, *Prog. Retinal Eye Res.*, 2006, **25**, 277–295.
- 10 R. F. Gariano and T. W. Gardner, Retinal angiogenesis in development and disease, *Nature*, 2005, **438**, 960–966.
- 11 M. I. Dorrell, E. Aguilar and M. Friedlander, Retinal vascular development is mediated by endothelial filopodia, a preexisting astrocytic template and specific R-cadherin adhesion, *Invest. Ophthalmol. Visual Sci.*, 2002, **43**, 3500–3510.
- 12 H. J. Junge, S. Yang, J. B. Burton, K. Paes, X. Shu, D. M. French, M. Costa, D. S. Rice and W. L. Ye, TSPAN12 Regulates Retinal Vascular Development by Promoting Norrin-but Not Wnt-Induced FZD4/beta-Catenin Signaling, *Cell*, 2009, **139**, 299–311.
- 13 Y. S. Wang, A. Rattner, Y. L. Zhou, J. Williams, P. M. Smallwood and J. Nathans, Norrin/Frizzled4 Signaling in Retinal Vascular Development and Blood Brain Barrier Plasticity, *Cell*, 2012, **151**, 1332–1344.
- 14 J. A. Stefater, I. Lewkowich, S. Rao, G. Mariggi, A. C. Carpenter, A. R. Burr, J. Q. Fan, R. Ajima, J. D. Molkenkin, B. O. Williams, M. Wills-Karp, J. W. Pollard, T. Yamaguchi, N. Ferrara, H. Gerhardt and R. A. Lang, Regulation of angiogenesis by a non-canonical Wnt-Flt1 pathway in myeloid cells, *Nature*, 2011, **474**, 511–515.
- 15 X. Ye, Y. S. Wang and J. Nathans, The Norrin/Frizzled4 signaling pathway in retinal vascular development and disease, *Trends Mol. Med.*, 2010, **16**, 417–425.
- 16 J. Stone and Z. Dreher, Relationship between astrocytes, ganglion cells and vasculature of the retina, *J. Comp. Neurol.*, 1987, **255**, 35–49.
- 17 T. L. Ling, J. Mitrofanis and J. Stone, Origin of retinal astrocytes in the rat: evidence of migration from the optic nerve, *J. Comp. Neurol.*, 1989, **286**, 345–352.
- 18 A. Uemura, S. Kusuhara, S. J. Wiegand, R. T. Yu and S. I. Nishikawa, Tlx acts as a proangiogenic switch by regulating extracellular assembly of fibronectin matrices in retinal astrocytes, *J. Clin. Invest.*, 2006, **116**, 369–377.
- 19 X. Ye, Y. S. Wang, H. Cahill, M. Z. Yu, T. C. Badesa, P. M. Smallwood, N. S. Peachey and J. Nathans, Norrin, Frizzled-4, and Lrp5 Signaling in Endothelial Cells Controls a Genetic Program for Retinal Vascularization, *Cell*, 2009, **139**, 285–298.
- 20 M. Hellstrom, L. K. Phng, J. J. Hofmann, E. Wallgard, L. Coultas, P. Lindblom, J. Alva, A. K. Nilsson, L. Karlsson, N. Gaiano, K. Yoon, J. Rossant, M. L. Iruela-Arispe, M. Kalen, H. Gerhardt and C. Betsholtz, Dll4 signalling through Notch1 regulates formation of tip cells during angiogenesis, *Nature*, 2007, **445**, 776–780.

- 21 M. Schmidt, K. Paes, A. De Maziere, T. Smyczek, S. Yang, A. Gray, D. French, I. Kasman, J. Klumperman, D. S. Rice and W. L. Ye, EGFL7 regulates the collective migration of endothelial cells by restricting their spatial distribution, *Development*, 2007, **134**, 2913–2923.
- 22 I. B. Lobov, R. A. Renard, N. Papadopoulos, N. W. Gale, G. Thurston, G. D. Yancopoulos and S. J. Wiegand, Delta-like ligand 4 (DII4) is induced by VEGF as a negative regulator of angiogenic sprouting, *Proc. Natl. Acad. Sci. U. S. A.*, 2007, **104**, 3219–3224.
- 23 J. Stone, A. Itin, T. Alon, J. Peer, H. Gnessin, T. Chanling and E. Keshet, Development of Retinal Vasculature Is Mediated by Hypoxia-Induced Vascular Endothelial Growth-Factor (Vegf) Expression by Neuroglia, *J. Neurosci.*, 1995, **15**, 4738–4747.
- 24 C. Kirbas and F. Quek, A review of vessel extraction techniques and algorithms, *ACM Comput. Surv.*, 2004, **36**, 81–121.
- 25 M. B. Vickerman, P. A. Keith, T. L. Mckay, D. J. Gedeon, M. Watanabe, M. Montano, G. Karunamuni, P. K. Kaiser, J. E. Sears, Q. Ebrahim, D. Ribita, A. G. Hylton and P. Parsons-Wingerter, VESGEN 2D: Automated, User-Interactive Software for Quantification and Mapping of Angiogenic and Lymphangiogenic Trees and Networks, *Anat. Rec.*, 2009, **292**, 320–332.
- 26 J. W. Hart, M. Goldbaum, B. Cote, P. Kube and M. R. Nelson, Automated measurement of retinal vascular tortuosity, *J. Am. Med. Inform. Assoc.*, 1997, 459–463.
- 27 E. Grisan, M. Foracchia and A. Ruggeri, A novel method for the automatic grading of retinal vessel tortuosity, *IEEE Trans. Med. Imaging*, 2008, **27**, 310–319.
- 28 D. Guidolin, B. Nico, G. Mazzocchi, A. Vacca, G. G. Nussdorfer and D. Ribatti, Order and disorder in the vascular network, *Leukemia*, 2004, **18**, 1745–1750.
- 29 P. Parsons-Wingerter, B. Lwai, M. C. Yang, K. E. Elliott, A. Milaninia, A. Redlitz, J. I. Clark and E. H. Sage, A novel assay of angiogenesis in the quail chorioallantoic membrane: Stimulation by bFGF and inhibition by angiotatin according to fractal dimension and grid intersection, *Microvasc. Res.*, 1998, **55**, 201–214.
- 30 M. E. Martinez-Perez, A. D. Hughes, A. V. Stanton, S. A. Thom, N. Chapman, A. A. Bharath and K. H. Parker, Retinal vascular tree morphology: A semi-automatic quantification, *IEEE Trans. Biomed. Eng.*, 2002, **49**, 912–917.
- 31 P. Parsons-Wingerter, U. M. Chandrasekharan, T. L. Mckay, K. Radhakrishnan, P. E. DiCorleto, B. Albarran and A. G. Farr, A VEGF(165)-induced phenotypic switch from increased vessel density to increased vessel diameter and increased endothelial NOS activity, *Microvasc. Res.*, 2006, **72**, 91–100.
- 32 W. Czech, W. Dzwiniel, S. Goryczka, T. Arodz and A. Z. Dudek, Exploring Complex Networks with Graph Investigator Research Application, *Comput. Inform.*, 2011, **30**, 381–410.
- 33 A. Stahl, K. M. Connor, P. Sapiuha, K. L. Willett, N. M. Krahe, R. J. Dennison, J. Chen, K. I. Guerin and L. E. Smith, Computer-aided quantification of retinal neovascularization, *Angiogenesis*, 2009, **12**, 297–301.
- 34 K. M. Connor, N. M. Krahe, R. J. Dennison, C. M. Aderman, J. Chen, K. I. Guerin, P. Sapiuha, A. Stahl, K. L. Willett and L. E. Smith, Quantification of oxygen-induced retinopathy in the mouse: a model of vessel loss, vessel regrowth and pathological angiogenesis, *Nat. Protocols*, 2009, **4**, 1565–1573.
- 35 K. Michielsen and H. De Raedt, Integral-geometry morphological image analysis, *Phys. Rep.*, 2001, **347**, 462–538.
- 36 M. Seul, L. O’Gorman and M. J. Sammon, *Practical algorithms for image analysis: description, examples, and code*, Cambridge University Press, Cambridge, New York, 2000, p. 295.
- 37 J. L. Starck, E. J. Candes and D. L. Donoho, The curvelet transform for image denoising, *IEEE Trans. Image Process.*, 2002, **11**, 670–684.
- 38 T. Geback and P. Koumoutsakos, Edge detection in microscopy images using curvelets, *BMC Bioinf.*, 2009, **10**, 75.
- 39 N. Hansen, S. D. Muller and P. Koumoutsakos, Reducing the time complexity of the derandomized evolution strategy with covariance matrix adaptation (CMA-ES), *Evol. Comput.*, 2003, **11**, 1–18.
- 40 H. Gerhardt, M. Golding, M. Fruttiger, C. Ruhrberg, A. Lundkvist, A. Abramsson, M. Jeltsch, C. Mitchell, K. Alitalo, D. Shima and C. Betsholtz, VEGF guides angiogenic sprouting utilizing endothelial tip cell filopodia, *J. Cell Biol.*, 2003, **161**, 1163–1177.
- 41 W. Y. Shen, M. Fruttiger, L. Zhu, S. H. Chung, N. L. Barnett, J. K. Kirk, S. Lee, N. J. Coorey, M. Killingsworth, L. S. Sherman and M. C. Gillies, Conditional Muller Cell Ablation Causes Independent Neuronal and Vascular Pathologies in a Novel Transgenic Model, *J. Neurosci.*, 2012, **32**, 15715–15727.
- 42 S. F. Hackett, S. Wiegand, G. Yancopoulos and P. A. Campochiaro, Angiopoietin-2 plays an important role in retinal angiogenesis, *J. Cell Physiol.*, 2002, **192**, 182–187.
- 43 U. F. O. Luhmann, J. H. Lin, N. Acar, S. Lammel, S. Feil, C. Grimm, M. W. Seeliger, H. P. Hammes and W. Berger, Role of the Norrie disease pseudoglioma gene in sprouting angiogenesis during development of the retinal vasculature, *Invest. Ophthalmol. Visual Sci.*, 2005, **46**, 3372–3382.
- 44 Q. Xu, Y. S. Wang, A. Dabdoub, P. M. Smallwood, J. Williams, C. Woods, M. W. Kelley, L. Jiang, W. Tasman, K. Zhang and J. Nathans, Vascular development in the retina and inner ear: Control by Norrin and Frizzled-4, a high-affinity ligand–receptor pair, *Cell*, 2004, **116**, 883–895.
- 45 I. Kovacevic, J. Hu, A. Siehoff-Icking, N. Opitz, A. Griffin, A. C. Perkins, A. L. Munn, W. Muller-Esterl, R. Popp, I. Fleming, B. Jungblut, M. Hoffmeister and S. Oess, The F-BAR protein NOSTRIN participates in FGF signal transduction and vascular development, *EMBO J.*, 2012, **31**, 3309–3322.
- 46 N. Ricard, S. Levet, D. Ciais, M. Subileau, C. Mallet, T. Zimmers, S. J. Lee, M. Bidart, J. J. Feige and S. Bailly, BMP9 and BMP10 are critical for postnatal retinal vascular remodeling, *Angiogenesis*, 2013, **16**, 256–257.
- 47 M. G. Watson, S. R. McDougall, M. A. J. Chaplain, A. H. Devlin and C. A. Mitchell, Dynamics of angiogenesis during murine retinal development: a coupled *in vivo* and *in silico* study, *J. R. Soc. Interface*, 2012, **9**, 2351–2364.
- 48 S. J. Wang, C. M. Sorenson and N. Sheibani, Attenuation of retinal vascular development and neovascularization during oxygen-induced ischemic retinopathy in Bcl-2^{-/-} mice, *Dev. Biol.*, 2005, **279**, 205–219.